



LAWRENCE
LIVERMORE
NATIONAL
LABORATORY

Adiabatic shear band formation in explosively driven AerMet-100 alloy cylinders

A. J. Sunwoo, R. Becker, D. M. Goto, T. J.
Orzechowski, H. K. Springer, C. K. Syn, J. Zhou

February 13, 2006

Scripta Materialia

Disclaimer

This document was prepared as an account of work sponsored by an agency of the United States Government. Neither the United States Government nor the University of California nor any of their employees, makes any warranty, express or implied, or assumes any legal liability or responsibility for the accuracy, completeness, or usefulness of any information, apparatus, product, or process disclosed, or represents that its use would not infringe privately owned rights. Reference herein to any specific commercial product, process, or service by trade name, trademark, manufacturer, or otherwise, does not necessarily constitute or imply its endorsement, recommendation, or favoring by the United States Government or the University of California. The views and opinions of authors expressed herein do not necessarily state or reflect those of the United States Government or the University of California, and shall not be used for advertising or product endorsement purposes.

This document was prepared as an account of work sponsored by an agency of the United States Government. Neither the United States Government nor the University of California nor any of their employees, makes any warranty, express or implied, or assumes any legal liability or responsibility for the accuracy, completeness, or usefulness of any information, apparatus, product, or process disclosed, or represents that its use would not infringe privately owned rights. Reference herein to any specific commercial product, process, or service by trade name, trademark, manufacturer, or otherwise, does not necessarily constitute or imply its endorsement, recommendation, or favoring by the United States Government or the University of California. The views and opinions of authors expressed herein do not necessarily state or reflect those of the United States Government or the University of California, and shall not be used for advertising or product endorsement purposes.

Adiabatic shear band formation in explosively driven AerMet-100 alloy cylinders

A.J. Sunwoo, R. Becker, D.M. Goto, T.J. Orzechowski, H.K. Springer, C.K. Syn, J. Zhou

Lawrence Livermore National Laboratory, PO Box 808, Livermore, CA 94550, United States

Abstract

Two differently heat-treated AerMet-100 alloy cylinders were explosively driven to fragmentation. Soft-captured fragments were studied to characterize the deformation and damage induced by high explosive loading. The characterization of the fragments reveals that the dominant failure mechanism appears to be dynamic fracture along adiabatic shear bands. These shear bands differ in size and morphology depending on the heat-treated conditions. Nanoindentation measurements of the adiabatic shear bands in either material condition indicate higher hardness in the bands compared to the matrix regions of the fragments.

Keywords: Dynamic deformation; Shear bands; Fractography; Nanoindentation

1. Introduction

High explosive (HE) driven cylinder tests have been commonly used to investigate the effect of this unique and complicated loading path on the failure and fragmentation of metals [1-6]. The material is first driven into compression as the shock passes through it and then undergoes tensile loading resulting in fracture and fragmentation. The present work examines the deformation and damage induced by this loading path on the AerMet-100 alloy. The fragments from the cylinders are collected in a “soft recovery” tank that mitigates secondary damage to the material. The fragments are then analyzed to determine the deformation and failure mechanisms that led to fracture.

The configuration used here is similar to that used by many researchers for several decades to investigate the behavior of ductile metals driven at high strain rates in order to understand the fracture and fragmentation characteristics of munitions. These experiments motivated and guided much of the seminal work on fragmentation behavior and modeling [1,2] and related microstructural mechanisms involved in the dynamic failure of metals [7].

AerMet-100 alloy is studied because of its high strength and toughness, and its wide range of applications ranging from armor to ordnance [8,9]. This study focuses on investigating HE drive induced shear band formation in the alloy and to provide microstructure information necessary to develop dynamic fracture models [10]. This report describes the microstructural observation related to the shear band formation.

This work was performed under the auspices of the U.S. Department of Energy by University of California, Lawrence Livermore National Laboratory under Contract W-7405-Eng-48.

2. Experimental Methods

AerMet-100 alloy was purchased in the form of normalized overaged, ground, round bar stock from Carpenter Technology Corporation (Heat #207470). The chemistry of the alloy in wt-% is 0.24 C, 2.99 Cr, 11.05 Ni 1.16 Mo, 13.32 Co and the balance is Fe. Hollow cylinders were produced from this bar stock using electrical discharge machining (EDM) and additional surface finish machining on both the inside and outside of the cylinders to produce a 0.4 μm finish. The cylinders are 20.32-cm long with a 5.08-cm outer diameter and a 0.3-cm wall thickness. Some of the cylinders are hardened using a heat-treatment schedule recommended by Carpenter Technology Corporation [9]. Post heat-treatment measurements showed that the cylinders maintained dimensional stability. Rockwell C hardness (HRC) increased from 40 to 55. Sound speed measurements in three orthogonal directions suggest the rod material is isotropic. The average longitudinal sound speeds increase from 5.77 km/s to 5.80 km/s, following the heat treatment. These values are consistent with published values [8]. Henceforth, the normalized overaged condition will be denoted as “as-received” (AR) and the age-hardened condition as “heat treated” (HT).

The hollow AerMet-100 alloy cylinders are loaded with a main charge of LX-17 HE. This HE has a Chapman-Jouguet pressure of 28 GPa. On one end of the cylinder, an LX-10 booster charge is mated to the LX-17 main charge to provide a near planar detonation of the main charge along the entire length of the cylinder. The detonation wave proceeded down the cylinder at a velocity of 7.7 km/s. The Gurney velocity for this configuration is 2.15 km/s corresponding to a terminal strain rate of $8.5 \times 10^4/\text{s}$. However, analyses of experiments using computer code simulations indicate that the material fragments before it reaches this strain rate [10].

To collect as many of the cylinder fragments as possible, a “soft-capture” tank comprising a low-density ($0.3\text{g}/\text{cm}^3$) foam box surrounded on the outside by water was fabricated. This capture tank was designed to slow the fragments down and ultimately stop them in a manner that mitigates further damage to the material by keeping the retarding pressure on the fragments below the ultimate tensile strength of the material.

The recovered fragments from the exploded cylinders were cleaned, dried, and stored in desiccant. Representative fragments were selected for microstructural characterization and analyses. Prior to cross-sectional metallography, the original inner and outer cylinder surfaces (identifiable on most fragments) were examined to characterize surface cracks and other deformation induced surface features. The fracture surfaces in both axial and circumferential directions were also examined to determine the failure modes. Fragments were sectioned and metallographic samples were prepared using standard sample preparation techniques. The polished surfaces were etched in a 5% nital solution to reveal the deformed microstructure. Samples of the virgin material were prepared in a similar manner. The deformed microstructure was examined with optical and scanning electron microscopy (SEM) imaging.

3. Results and discussion

The microstructures of the AR and HT AerMet-100 alloy are shown in Fig. 1. The AR microstructure contains martensite and randomly embedded incoherent $1.5 \pm 0.8 \mu\text{m}$ diameter spherical inclusions. Energy dispersive X-ray spectroscopy indicates that the micron-sized inclusions are composed of As, Ce and La. A detailed analysis (performed on a recovered

fragment from an AR cylinder) indicates an areal density of these spherical inclusions of approximately $40/\text{mm}^2$. This areal density corresponds to a volume density of approximately $250/\text{mm}^3$ and a mean inclusion spacing of 0.17 mm. After the heat treatment, the martensite boundaries are homogeneously decorated with precipitates. The coherent submicron sized grain boundary precipitates are identified as M_2C carbides [11]. These carbides are the primary contributors to increased hardness observed in the heat-treated sample.

The fragments recovered from either the AR or HT cylinders typically have a fragment length-to-width ratio of approximately five. The average fragment length is 16 mm while the average fragment width is about 3 mm. However the spread in each of these quantities is rather large. The SEM fractography of a HT fragment is shown in Fig. 2. The fracture surfaces defining the ends of the long dimension of the fragment reveal typical tensile failure, characterized by a mixture of very fine and enlarged dimples caused by various sized inclusions. Along the fragment length, the fracture surface is inclined at $\pm 45^\circ$ to the inner or outer surface; but this angle can abruptly change from $+45^\circ$ to -45° on a given surface. Hence, these shear-fracture surfaces can either be parallel to each other, resulting in a parallelogram shaped cross-section; or the fracture surfaces can be anti-parallel, resulting in a trapezoidal or triangular cross section. These surfaces show both equiaxed and teardrop shaped ductile dimples, characteristic of Mode I and/or Mode II crack growth [12].

The original inner and outer surfaces of the fragment show a hierarchy of deformation-induced features, ranging from very small surface perturbations to small cracks to complete fracture. These features are aligned along the long dimension of the fragment. The smallest scale surface perturbations appear to be surface roughening and clearly defined surface steps or discontinuities. These steps are typically several microns deep, have axial lengths on the order of a millimeter and average separations on the order of 200 μm . Some of these steps are associated with adiabatic shear bands (ASBs) that penetrate into the fragment interior [13-15]. On a larger scale, longitudinal cracks have axial lengths on the order of a couple of millimeters and inter-crack separations on the order of 1 mm. They are oriented along the axis of the cylinder in the same direction as the shear fracture surface, as shown in Fig. 3.

Examining the irregular surfaces that define the narrow dimension of the fragment, *i.e.*, its width, we surmise that some of these longitudinal cracks link to form a single large crack, as shown in Fig. 4a. A cross-section orthogonal to the long dimension of this particular HT cylinder fragment reveals that occasionally a “parallel” and “anti-parallel” crack meet so that the fracture surface changed its cross-sectional shape from a parallelogram to a trapezoid. The damage induced on the surface and within the fragment is clearly seen in Figs. 4b-4d. Larger surface defects that penetrate into the material up to hundreds of microns transition into very narrow and well-defined deformation bands; see Figs. 4c and 4d. These narrow deformation bands are identified as ASB [13-21]. The width of the deformation is highly localized—approximately 1 μm . The material accumulates shear strains on the order of 3 or more in this region. Cracks that have propagated into but not through the material constitute the largest surface defects observed; see Figs. 4b and 4d. These cracks terminate in the fragment interior, transitioning into ASBs.

The AR cylinder fragments exhibit similar deformation features as those observed in HT cylinder fragments. However, ASBs found in this softer material are notably wider, on the order of 1.5 - 5 μm . The larger widths and width variations associated with shear bands found in the AR material are the result of the shear bands being not as defined as those found in the HT material. The deformation gradient between the matrix and shear band is less pronounced in the

AR material than in the HT material, such that a transition region of increasingly sheared material is clearly observable in the former; see Fig. 5.

Differences between shear bands found in the AR and HT materials have also been observed in other high strength steels [19-21]. Cho et al. [19] observed similar diffuse shear bands in a softer (HRC44) AISI 4340 steel and more distinct, narrower bands in a harder (HRC55) 4340 steel. These investigators concluded that the shear bands with sharp edges (more defined edges) formed by deformation induced phase transformation within the shear band. The shear bands in the softer material, in which plastic flow lines are clearly visible in the material region adjacent to the shear band, did not involve a phase transformation. The phase transformation is induced by localized strain energy work (heating) within the shear band, which is more probably to occur in a harder material due to the high flow strength.

Results of nanoindentation hardness (H_n) measurements within the ASB of both the AR and HT material suggest both shear bands experienced significant strain hardening. The H_n of the ASB in the AR material is approximately 33% higher than the matrix hardness. The H_n of the ASB in the HT material is approximately 17% higher than the matrix. The larger increase in hardness measured in the AR material suggests that less of the strain hardening caused by the intense localized deformation is recovered due to the adiabatic heating than for the HT material. However, if both materials experience some degree of deformation induced phase transformation, the resulting phase may be harder than the starting phase; conventional hardening in the AerMet-100 alloy is the result of heat treatment.

4. Conclusions

Explosively driven AerMet-100 cylinders, both AR and HT, are highly susceptible to strain localization induced adiabatic shear band formation. Crack nucleation and growth occurs along these shear bands. Although numerous cracks form, most terminate in the material interior at shear band intersections. Nanoindentation measurements of the adiabatic shear bands in both materials indicate higher hardness compared to the matrix regions of the fragments.

Acknowledgements

J. Go and E. M. Sedillo are gratefully acknowledged for their assistance in the metallographic analysis. This work was performed under the auspices of the U.S. Department of Energy by University of California, Lawrence Livermore National Laboratory under Contract W-7405-Eng-48.

References

- [1] Mott NF. Proc. Royal Society A189, London; 1947, p. 300.
- [2] Taylor GI. The Fragmentation of Tubular Bombs, Aero. Mech. Proj. Expl., Vol. III: Cambridge; 1963. p. 387.
- [3] Grady DE, Hightower MM Shock Waves and High-Strain-Rate Phenomena in Metals. New York: Marcel Dekker; 1992, p. 713.
- [4] Banks EE. J. Inst. Metals 1968;96:375.
- [5] Olive F, Nicaud A, Marilleau J, Loichit R. Proc. 2nd Conf. Mechanical Properties of Materials at High Rates of Strain, Oxford: 1979. p. 242.

- [6] Mock W, Holt WH. *J. Applied Physics* 1983;54:2344.
- [7] Shockey DA, Erlich DC. *Shock Waves and High-Strain-Rate Phenomena in Metals*. New York: Plenum Press; 1981. p. 249.
- [8] Chhabildas LC, Thornhill TF, Reinhart WD, Kipp ME, Reedal DR, Wilson LT, Grady D.E. *Int. J. Impact Eng.* 2001;26:77.
- [9] *AerMet-100 Alloy Data*. Carpenter Specialty Alloys 1995.
- [10] Goto DM, Becker R, Orzechowski TJ, Springer HK, Sunwoo AJ, Syn CK UCRL-TR-213016 2005:305.
- [11] Ayer R, Machmeier P. *Met. Mater. Trans. A* 1998;29A:903.
- [12] Hertzberg RW, *Deformation and Fracture Mechanics of Engineering Materials*, 3rd ed. New York: Wiley; 1989. p. 277.
- [13] Me-Bar Y, Shechtman D. *Mater. Sci. Eng* 1983; 58:181.
- [14] Lee CG, Park WJ, Lee S, Shin KS. *Met. Mater. Trans. A* 1998;29A: 477.
- [15] Duan ZQ, Li SX, Huang DW. *Fatig. Fract. Eng. Mater. Struct.* 2003;29:1119.
- [16] Meyers M, Pak H-R. *Acta metall.* 1986;34:2493.
- [17] Cho K, Lee S, Nutt SR, Duffy J. *Acta metall*, 1992;41:923.
- [18] Marchand A, Duff, J. J. *Mech. Phys. Solids* 1988;36:251.
- [19] Cho K, Chi YC, Duffy J. *Metall. Trans. A* 1990;21A:116.
- [20] Hutchenson JW. *Scripta mater.* 1984;18:421.
- [21] Timothy SP. *Acta metall.* 1987;35:301.

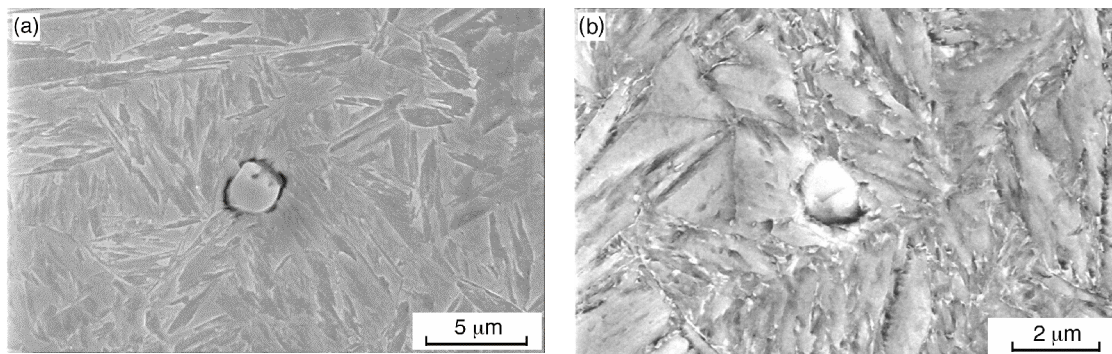


Fig. 1. SEM images of (a) AR and (b) HT AerMet-100 alloy showing the inclusions and precipitates in martensite boundaries after the heat treatment.

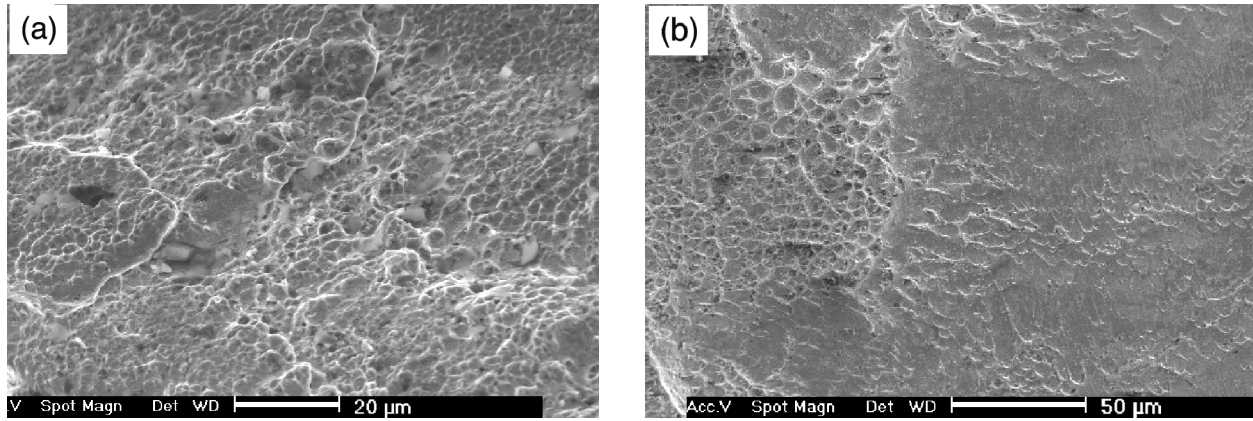


Fig. 2. SEM fractography of a HT fragment shown in (a) end of long dimension and (b) 45° shear.

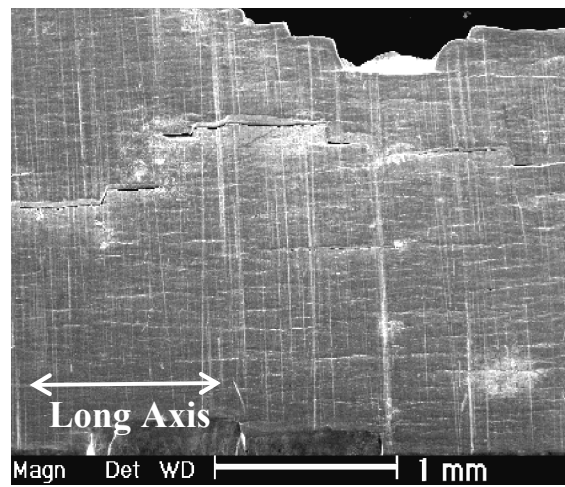
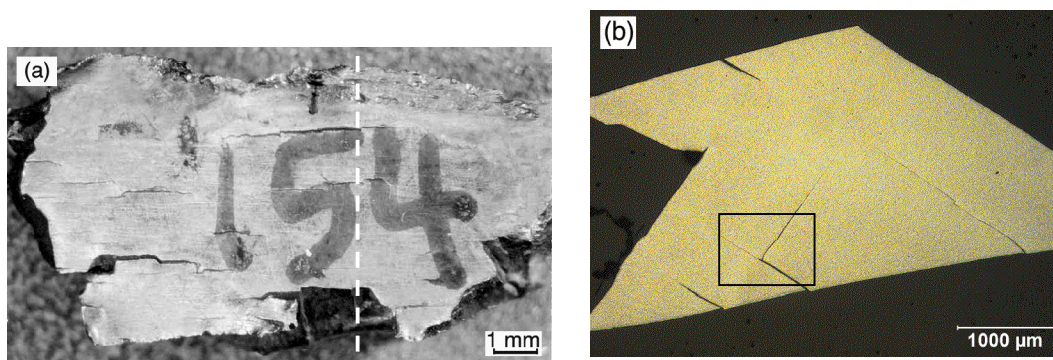


Fig. 3. SEM image of the original outer surface of a HT fragment (#83) showing the hierarchy of deformation. The vertical lines are the machining marks.



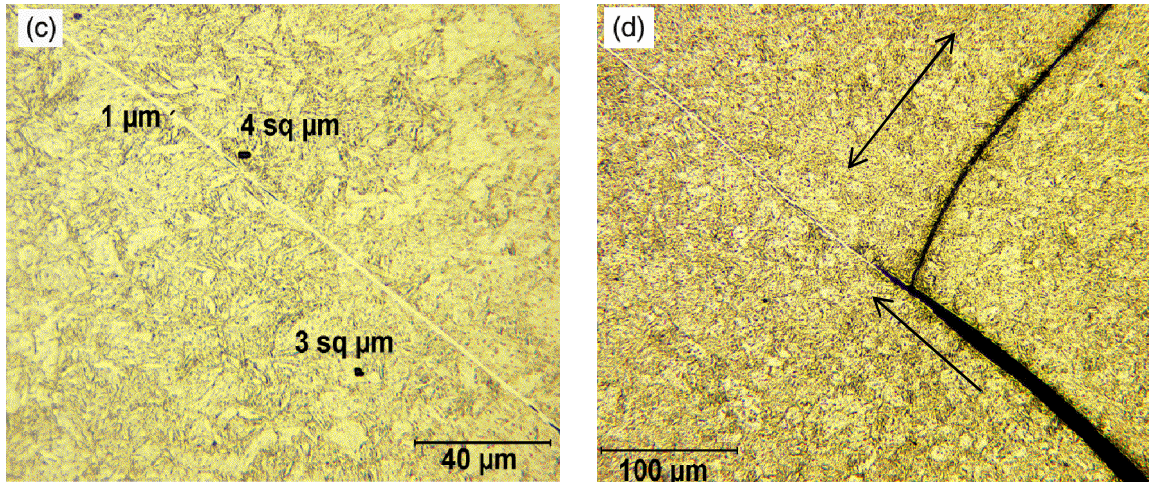


Fig. 4. Optical images of (a) HT fragment, (b) orthogonal cross-sectional view from a dashed line, (c) adiabatic shear band ($1\ \mu\text{m}$) and area of the microvoids, and (d) from a boxed region showing interaction between ASB and cracks. Arrows indicate the directions of crack propagation and shear band in (d).

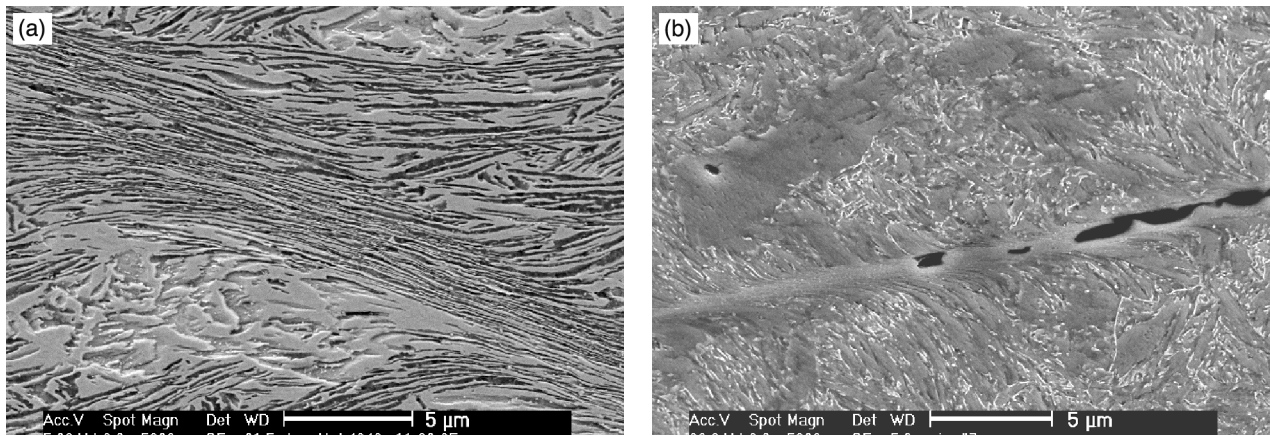


Fig. 5. SEM images of (a) AR fragment #9 where the width of the shear bands lies between 1.5 and $5\ \mu\text{m}$, and (b) HT fragment #154 where the width of the shear bands is less than $1.5\ \mu\text{m}$.